

Dust storm-enhanced gravity wave activity in the Martian thermosphere observed by MAVEN and implication for atmospheric escape

Erdal Yiğit¹, Alexander S. Medvedev², Mehdi Benna^{3,4}, Bruce M. Jakosky⁵

¹George Mason University, Department of Physics and Astronomy.

²Max Planck Institute for Solar System Research, Göttingen, Germany.

³University of Maryland Baltimore County, Baltimore, MD, USA.

⁴Solar System Exploration Division, NASA Goddard Space Flight Center, Greenbelt, MD, USA.

⁵Laboratory for Atmospheric and Space Physics, University of Colorado, CO, USA.

Key Points:

- Thermospheric gravity wave activity doubles during the dust storm.
- Gravity wave induced density fluctuations in the thermosphere are up to 40% during the peak storm phase.
- Gravity waves significantly increase Hydrogen escape flux by modulating temperature fluctuations.

arXiv:2101.07698v1 [physics.space-ph] 19 Jan 2021

Abstract

Lower atmospheric global dust storms affect the small- and large-scale weather and variability of the whole Martian atmosphere. Analysis of the CO₂ density data from the Neutral Gas and Ion Mass Spectrometer instrument (NGIMS) on board NASA's Mars Atmosphere Volatile Evolution (MAVEN) spacecraft show a remarkable increase of GW-induced density fluctuations in the thermosphere during the 2018 major dust storm with distinct latitude and local time variability. The mean thermospheric GW activity increases by a factor of two during the storm event. The magnitude of relative density perturbations is around 20% on average and 40% locally. One and a half months later, the GW activity gradually decreases. Enhanced temperature disturbances in the Martian thermosphere can facilitate atmospheric escape. For the first time, we estimate that, for a 20% and 40% GW-induced disturbances, the net increase of Jeans escape flux of hydrogen is a factor of 1.3 and 2, respectively.

Plain Language Summary

Atmospheric gravity waves play an important dynamical and thermodynamical role in coupling the different atmospheric layers, especially on Earth and Mars. We study the effects of a planet-encircling major dust storm on thermospheric gravity wave activity and estimate for the first time a potential influence of gravity waves on atmospheric escape on Mars. Gravity activity measured in terms of relative density fluctuations increases by a factor of two during the peak phase of the storm. We show that larger-amplitude gravity waves facilitate atmospheric escape of hydrogen from Mars' upper atmosphere. For 40% gravity wave-induced relative disturbances of temperature, the net escape rate doubles.

1 Introduction

Dust greatly impacts the dynamics and thermodynamics of the entire Martian atmosphere (Haberle et al., 1982; Zurek & Martin, 1993; Bell et al., 2007; Cantor, 2007; Clancy et al., 2010; Heavens et al., 2011; Medvedev et al., 2013; Jain et al., 2020; Wu et al., 2020; Liuzzi et al., 2020). During storms, regolith particles are raised from the surface and modify temperature by absorbing more solar radiation within the atmosphere and obstructing heating of the lowermost layers (Gierasch & Goody, 1972; Rafkin, 2009). Once dust is airborne, sedimentation may take up to several months. Depending on the scale, storms can be regional or global with wide-reaching implications for the planetary climate.

Dust storms affect circulation at all scales, in particular the atmospheric gravity wave (GW) activity. GWs (or buoyancy waves) are ubiquitous features of all planetary atmospheres (e.g., see recent reviews of Yiğit & Medvedev, 2019; Medvedev & Yiğit, 2019). They have been extensively studied on Earth since the 1960s, when their essential role in coupling atmospheric layers was recognized. On Mars, GWs have been observed by a number of satellites (Fritts et al., 2006; Tolson et al., 2007; Yiğit et al., 2015; England et al., 2017; Jesch et al., 2019; Vals et al., 2019; Siddle et al., 2019) and studied with numerical models (Parish et al., 2009; Medvedev et al., 2013; Walterscheid et al., 2013; Imamura et al., 2016; Yiğit et al., 2018; Kuroda et al., 2019). The main mechanism by which GWs affect the dynamics and state of the atmosphere is transporting energy and momentum from denser lower levels and depositing them in the thinner upper atmosphere. The latter is also the region where atmospheric escape takes place (Walterscheid et al., 2013; Chaffin et al., 2018), however the impact of GWs on the escape rate has not been considered observationally before, to the best of our knowledge.

Thermospheric response to global dust storms (GDS) have been extensively studied during the major event of 2018. In particular, Jain et al. (2020) and Elrod et al. (2020) characterized large-scale thermospheric effects of the GDS. Recently, based on the Ar measurements with the Neutral Gas and Ion Spectrometer (NGIMS) instrument on board the Mars Atmosphere Volatile Evolution Mission (MAVEN) orbiter, Leelavathi et al. (2020) reported on the increase

of GW activity during the storm of 2018 in the thermosphere. In our paper, we also quantify thermospheric GW activity during different phases of the planet encircling dust storm that commenced on 1 June 2018 using NGIMS' measurements of CO₂ and discuss possible implications for atmospheric escape.

2 Materials and Methods

2.1 Data Sets Analyzed

For the analysis of the GW activity before and during the planet-encircling global dust storm, we consider data from the NGIMS instrument onboard the MAVEN spacecraft from 1 May 2018 till 30 September 2018, corresponding to $L_s = 167^\circ - 259.6^\circ$ in Martian Year (MY) 34. In the analysis to be presented we also compare the dust-storm GW activity in MY34 with a low-dust period one Martian year earlier. For this, the low-dust period in MY 33 with solar longitudes $L_s = 171.7^\circ - 191.6^\circ$ (20 June-25 July 2016) is compared with a representative dust storm period in MY 34, $L_s = 202.8^\circ - 224.2^\circ$ (1 July-5 August 2018), when MAVEN had comparable latitude and local time coverage. The details of the data used and orbital coverage are provided in the supporting information and figures.

2.2 Observational Analysis of Wave Activity

Calculation of the GW fluctuations requires information on the background field. For this, we use a 7-th order polynomial fit to the logarithm of the CO₂ (carbon dioxide) density profiles to determine the mean field. Polynomial fit technique has been used in a number of previous studies of GWs on Mars (Yiğit et al., 2015; England et al., 2017; Siddle et al., 2019) and Earth (Randall et al., 2017). In order to calculate the GW-induced fluctuations we subtract the background mean density (i.e., the polynomial fit) from the instantaneous measurements to determine the GW disturbance as:

$$\rho' = \rho - \bar{\rho}, \quad (1)$$

where the $\bar{\rho}$ is the background (polynomial fitted density) and ρ is the measured (instantaneous) CO₂ density. The relative density perturbation in percentage is then given by dividing the density fluctuations by the background mean, $\rho'/\bar{\rho}$, and multiplying by 100. This analysis is used for each orbit, including the inbound and the outbound pass.

In order to evaluate the variation of the GW activity for the period of one month before the onset of the storm to the end phases (1 May 2018 till 30 September 2018), we first organize all 683 orbits in ~ 15 -day (~ 15 -sol) intervals. Then 15-day mean GW-induced relative density fluctuations, $\overline{\rho'/\bar{\rho}}$, are calculated from the average of data points within each bin as a function of altitude, longitude, latitude, and local time as presented in Figure 1, using 5 km, 30°, 5°, and 1 hour bins, respectively. For the comparison of MY34 dust-storm period (1 July-5 August 2018) to MY33 low-dust period (20 June-25 July 2016) presented in Figure 2, we focused on the data between 160 and 200 km, and binned them in terms of 5 km, 20° longitude, 5° latitude, and 0.5 hour bins. This for example means that data point at the altitude level 160 km represents the average value for the bin from 160-165 km. The typical uncertainty in the mean GW activity is about 0.26–0.7%. The details of the GW analysis and the uncertainty are discussed in the supporting material and figures.

3 Results

Variations of the GW-induced CO₂ relative density fluctuations before and during the storm are shown in Figure 1. The average fluctuations increase from 8-12% before the onset (1 June 2018) and rapidly increase afterwards, peaking with $\sim 40\%$ between 1-16 July ($L_s = 202.8^\circ - 211.9^\circ$) around 190-195 km. The GW activity increases at all thermospheric heights (panel a), but the maximum occurs between ~ 165 -205 km. Panels (b-d) show the longitude,

latitude, and local time variations of GW activity during the same period, focusing on the region between 165-185 km. Enhanced activity is systematically seen there in all analyses. During this period, MAVEN's observations sampled low latitudes (15°S – 20°N) and local nighttime (4-6 h). They demonstrate some difference in GW activity with larger values in the low-latitude southern (spring) hemisphere than the low-latitude northern hemisphere. MAVEN's orbit and coverage change in latitude and local time over the analyzed period (see supplementary Figure S1). From the pre-storm period toward the peak of the GDS, the spacecraft coverage moves from southern midlatitudes (45°S – 25°S) to equatorial latitudes (15°S – 20°N) and from local times 9-13 h to 4-6 h. These changes should be accounted for in order to isolate them from dust-induced effects.

For that, we consistently compared the GW activity during the 2018 GDS against measurements for low-dust conditions one Martian year earlier. MAVEN's coverage changed with L_s , latitude and local time due to specifics of the orbit. We identified two periods with similar seasonal and spatial orbit characteristics: 20 June-25 July 2016 (MY 33, $L_s = 171.7^{\circ} - 191.6^{\circ}$) and 1 July-6 August 2018 (MY 34, $L_s = 202.8^{\circ} - 224.2^{\circ}$) (see supplementary information). Figure 2 shows the altitude, longitude, latitude and local time variations of GW activity during these two periods. Similar to Figure 1, averaging over the height interval 165-185 km has been performed. It is seen that GW activity is about two times larger during the storm. The southern hemisphere (SH) values are larger than those in the northern hemisphere (NH) for both the low-dust and dusty conditions. Figure 3 shows another perspective of how GW activity increases as a consequence of the GDS, presented in terms of global distributions of wave-induced density fluctuations during the chosen periods. Here, we binned the nighttime (local times 1.5-4.5 h) data between 165-185 km in terms of latitude and longitude. The effect of the storm on the GWs is remarkable: the activity is around 8-10% under low-dust conditions and increases to more than 20% globally and even 40% locally.

4 Discussion

4.1 Mechanism of Dust-Induced Gravity Wave Enhancement

The observed enhancement of GW activity in the upper atmosphere during the dust storm agrees well with the results of Leelavathi et al. (2020), but is quite unexpected. Since the gravity wave energy and momentum flux are proportional to the square of the wave amplitude, the increase in observed amplitude is, in fact, even higher in terms of these dynamically important quantities. An overall effect of storms on the lower atmosphere is the convective (Figure 1c of Kuroda et al., 2020) and baroclinic (Figure 2 of Kuroda et al., 2007) stabilization of the circulation: smaller lapse rates impede development of convection, and intensified zonal jets inhibit formation of larger-scale weather disturbances. This effectively suppresses the major mechanisms of GW generation in the lower atmosphere. Observations by Mars Climate Sounder provided evidence of a reduction of GW activity below 30 km by several times during the 2018 GDS (Heavens et al., 2020). Airborne aerosol particles do not rise above ~ 70 km. Why does the wave activity in the upper atmosphere increase then?

In the absence of other indications favoring in-situ wave generation, a plausible explanation is related to changes in the upward propagation of GWs. The latter primarily depends on the background winds and wave dissipation, such as nonlinear breaking and molecular diffusion (Hickey & Cole, 1988; Yiğit et al., 2008; Parish et al., 2009; Hickey et al., 2015). GW harmonics are absorbed by the mean flow, when their horizontal phase velocity approaches the ambient wind speed. Large local vertical gradients within a wave make harmonics prone to break-down and/or enhanced dissipation. During dust storms, the middle atmosphere circulation undergoes substantial changes due to the storm-induced radiative heating, which in turn modulate upward propagation and dissipation of GWs. The observed increase in thermospheric GW activity indicates that GW harmonics encounter more favorable propagation conditions during the dust storm. High-resolution simulations have demonstrated that the middle atmospheric GW activity increases despite the reduction in the lower atmosphere (Kuroda et

al., 2020), thus supporting this hypothesis. Although the details of this mechanism are not fully understood, it provides evidence for yet another consequence of Martian dust storms: they facilitate vertical coupling between atmospheric layers.

The increase of GW activity is even more unexpected in view of the recent finding that wave amplitudes observed by NGIMS typically decrease in proportion to the upper thermospheric temperature (England et al., 2017; Terada et al., 2017; Vals et al., 2019). The mechanism that likely controls such behavior is wave saturation due to convective instability, which permits larger amplitudes when the atmosphere is colder. However, the thermosphere warms during the 2018 dust storm event (Jain et al., 2020), which would imply weaker GW activity contrary to our results.

4.2 Gravity Waves and Atmospheric Escape

The observed enhancement of GW activity in the upper atmosphere during the MY34 GDS has far-reaching implications for the state as well as short- and long-term evolution of the Martian atmosphere. Recent ExoMars Trace Gas Orbiter observations reported a sudden increase of water vapor in the middle atmosphere during the storm, which was delivered there from below by the thermally-enhanced meridional circulation (Vandaele et al., 2019; Fedorova et al., 2020). This finding was further supported by numerical general circulation modeling (Shaposhnikov et al., 2019; Neary et al., 2020). It was suggested that this mechanism has likely governed the escape of water to space over geological time scales (Fedorova et al., 2020). The reported increase of GW activity at the very top of the atmosphere indicates that the waves not only contribute to the intensification of the transport, but can also directly boost the escape of hydrogen - a product of water photo-dissociation. The dominant process of its losses on Mars - Jeans escape - strongly depends on air temperature, which determines Maxwellian velocities of molecules.

Large density disturbances within the GW field imply similarly large variations of temperature: by 50 K on average and 100 K locally, based on relative density fluctuations and 250 K exobase mean temperature (Medvedev et al., 2016). In order to illustrate the net increase of atmospheric losses induced by temperature variations associated with GWs, we consider the escape flux ϕ at the exobase. It is given by the expression (Chaffin et al., 2018)

$$\phi = n \frac{v_{mp}}{2\sqrt{\pi}} (1 + \lambda) e^{-\lambda}, \quad v_{mp} = \sqrt{\frac{2kT}{m}}, \quad \lambda = \frac{GMm}{kRT}, \quad (2)$$

where n is the exobase density, T is the exobase temperature, v_{mp} is the most probable Maxwell-Boltzmann velocity, λ is the escape or Jeans parameter, k is the Boltzmann constant, R is the exobase radius, m is the mass of the hydrogen atom, M is the planetary mass, and G is the universal gravitational constant. The parameter $\lambda \approx 6$ at $T = 250$ K at the Martian exobase (Lammer et al., 2005). The ratios of fluxes for wave-disturbed and undisturbed temperature $\frac{\phi(T+\delta T)}{\phi(T)}$ for sinusoidally varying temperature disturbance δT are shown in Figure 4 for two characteristic values: the reported 20% (on average) and 40% (locally). It is seen that the hydrogen escape flux increases by a factor of more than 2.5 and 5.5 at the peak of the positive phase for 20%- and 40% disturbances of temperature, respectively. The difference grows with the amplitude of fluctuations. Since the enhancement on the positive phase exceeds the reduction on the negative one, the net flux (integrated over the entire wave phase, the area shown with shades) also increases. For a 20% and 40% disturbances of temperature, the increase of the net escape flux is of 1.3 and 2, respectively. Note that this estimate does not account for wave-induced displacements of air parcels (pressure variations), which also contribute to the escape flux enhancement.

Ordinarily, GW activity would be strongest when the thermosphere is coolest and vice versa, limiting escape as one effect canceled the other. However, dust storms reverse this paradigm, enabling larger wave amplitudes in a warmer background thermosphere. If the impact of the vertical water transport is considered, dust storms really represent a triple threat for atmospheric

losses. Constraining the role of GWs in both transport and escape can thus help with quantifying the processes, which have made Mars a dry planet.

5 Summary and Conclusions

Gravity wave-induced disturbances of CO₂ density obtained from the NGIMS instrument on board MAVEN in the Martian thermosphere have been compared for two distinctive periods with the most close orbital coverage around the mid-year equinoxes: one during the dustless Martian Year (MY) 33 and the other in the midst of the MY34 global dust storm. For the first time, the net increase in Jeans escape due to GW-induced fluctuations is estimated during the storm. The main results are listed below.

1. GW activity approximately doubles during the dust storm. This estimate quantitatively agrees with that of Leelavathi et al. (2020), who considered Ar density fluctuations over a half-year period.
2. The magnitude of relative density perturbations is around 20% on average and 40% locally.
3. The estimated net increase of Jeans escape flux of hydrogen is a factor of 1.3 and 2 for a 20% and 40% GW-induced disturbances of temperature, respectively.

From a technological point of view, large GW-induced thermospheric density disturbances during dust storms can endanger spacecraft entries into the atmosphere, similar to aircraft that encounter bumpiness when flying over hills and mountains, and occasionally due to clear air turbulence. In all these cases, GWs are involved, and their forecasting is important and challenging.

Acknowledgments

The NGIMS level 2, version 8 data supporting this article are publicly available at

https://atmos.nmsu.edu/data_and_services/atmospheres_data/MAVEN/ngims.html

References

- Bell, J. M., Bougher, S. W., & Murphy, J. R. (2007). Vertical dust mixing and the inter-annual variations in the Mars thermosphere. *J. Geophys. Res.*, *112*. doi: 10.1029/2006JE002856
- Cantor, B. A. (2007, January). MOC observations of the 2001 Mars planet-encircling dust storm. *Icarus*, *186*(1), 60–96. doi: 10.1016/j.icarus.2006.08.019
- Chaffin, M. S., Chaufray, J. Y., Deighan, J., Schneider, N. M., Mayyasi, M., Clarke, J. T., ... Jakosky, B. M. (2018). Mars H Escape Rates Derived From MAVEN/IUVS Lyman Alpha Brightness Measurements and Their Dependence on Model Assumptions. *J. Geophys. Res. Planets*, *123*(8), 2192–2210. doi: <https://doi.org/10.1029/2018JE005574>
- Clancy, R. T., Wolff, M. J., Whitney, B. A., Cantor, B. A., Smith, M. D., & McConnochie, T. H. (2010). Extension of atmospheric dust loading to high altitudes during the 2001 Mars dust storm: MGS TES limb observations. *Icarus*, *207*(1), 98–109. doi: 10.1016/j.icarus.2009.10.011
- Elrod, M. K., Bougher, S. W., Roeten, K., Sharrar, R., & Murphy, J. (2020). Structural and Compositional Changes in the Upper Atmosphere Related to the PEDE-2018 Dust Event on Mars as Observed by MAVEN NGIMS. *Geophys. Res. Lett.*, *47*(4). doi: 10.1029/2019GL084378
- England, S. L., Liu, G., Yiğit, E., Mahaffy, P. R., Elrod, M., Benna, M., ... Jakosky, B. (2017). MAVEN NGIMS observations of atmospheric gravity waves in

- the Martian thermosphere. *J. Geophys. Res. Space Physics*, 2310–2335. doi: 10.1002/2016JA023475
- Fedorova, A. A., Montmessin, F., Korablev, O., Luginin, M., Trokhimovskiy, A., Belyaev, D. A., . . . Wilson, C. F. (2020). Stormy water on Mars: The distribution and saturation of atmospheric water during the dusty season. *Science*, 367(6475), 297–300. doi: 10.1126/science.aay9522
- Fritts, D. C., Wang, L., & Tolson, R. H. (2006). Mean and gravity wave structures and variability in the Mars upper atmosphere inferred from Mars global surveyor and Mars odyssey aerobraking densities. *J. Geophys. Res.*, 111. doi: 10.1029/2006JA011897
- Gierasch, P. J., & Goody, R. M. (1972). The effect of dust on the temperature of the Martian atmosphere. *J. Atmos. Sci.*, 29.
- Haberle, R. M., Leovy, C. B., & Pollack, J. B. (1982). Some effects of global dust storms on the atmospheric circulation of Mars. *Icarus*, 50(2). doi: 10.1016/0019-1035(82)90129-4
- Heavens, N., Kass, D. M., Kleinböhl, A., & Schofield, J. T. (2020). A multiannual record of gravity wave activity in Mars's lower atmosphere from on-planet observations by the Mars Climate Sounder. *Icarus*, 341, 113630. doi: 10.1016/j.icarus.2020.113630
- Heavens, N., McCleese, D., Richardson, M., Kass, D., Kleinböhl, A., & Schofield, J. (2011). Structure and dynamics of the Martian lower and middle atmosphere as observed by the Mars Climate Sounder: 2. Implications of the thermal structure and aerosol distributions for the mean meridional circulation. *J. Geophys. Res. Planets*, 116(E1).
- Hickey, M. P., & Cole, K. D. (1988). A numerical model for gravity wave dissipation in the thermosphere. *J. Atmos. Terr. Phys.*, 50, 689–697.
- Hickey, M. P., Walterscheid, R. L., & Schubert, G. (2015). A full-wave model for a binary gas thermosphere: Effects of thermal conductivity and viscosity: Full-Wave Model for a Binary Gas. *J. Geophys. Res. Space Physics*, 120(4), 3074–3083. doi: 10.1002/2014JA020583
- Imamura, T., Watanabe, A., & Maejima, Y. (2016). Convective generation and vertical propagation of fast gravity waves on Mars: One- and two-dimensional modeling. *Icarus*, 267, 51–63. doi: 10.1016/j.icarus.2015.12.005
- Jain, S. K., Bougher, S. W., Deighan, J., Schneider, N. M., González Galindo, F., Stewart, A. I. F., . . . Pawlowski, D. (2020). Martian Thermospheric Warming Associated With the Planet Encircling Dust Event of 2018. *Geophys. Res. Lett.*, 47(3). doi: 10.1029/2019GL085302
- Jesch, D., Medvedev, A. S., Castellini, F., Yiğit, E., & Hartogh, P. (2019). Density Fluctuations in the Lower Thermosphere of Mars Retrieved From the ExoMars Trace Gas Orbiter (TGO) Aerobraking. *Atmosphere*, 10(10), 620. doi: 10.3390/atmos10100620
- Kuroda, T., Medvedev, A. S., Hartogh, P., & Takahashi, M. (2007). Seasonal changes of the baroclinic wave activity in the northern hemisphere of Mars simulated with a gcm. *Geophys. Res. Lett.*, 34(9). doi: https://doi.org/10.1029/2006GL028816
- Kuroda, T., Medvedev, A. S., & Yiğit, E. (2020). Gravity Wave Activity in the Atmosphere of Mars During the 2018 Global Dust Storm: Simulations With a High-Resolution Model. *J. Geophys. Res. Planets*, 125(11). doi: 10.1029/2020JE006556
- Kuroda, T., Yiğit, E., & Medvedev, A. S. (2019). Annual cycle of gravity wave activity derived from a high-resolution martian general circulation model. *J. Geophys. Res. Planets*, 124(6), 1618–1632. doi: 10.1029/2018JE005847
- Lammer, H., Selsis, F., Penz, T., V. Amerstorfer, U., Lichtenegger, H. I. M., Kolb, C., & Ribas, I. (2005). 2 atmospheric evolution and the history of water on mars. In T. Tokano (Ed.), *Water on mars and life* (pp. 25–43). Berlin, Heidelberg: Springer Berlin Heidelberg. doi: 10.1007/978-3-540-31538-4_2
- Leelavathi, V., Venkateswara Rao, N., & Rao, S. V. B. (2020). Interannual variability of atmospheric gravity waves in the Martian thermosphere: Effects of the 2018 planet-encircling dust event. *J. Geophys. Res. Planets*, 125(12), e2020JE006649. doi: 10.1029/2020JE006649
- Liuzzi, G., Villanueva, G. L., Crismani, M. M., Smith, M. D., Mumma, M. J., Daerden,

- F., ... Patel, M. R. (2020). Strong Variability of Martian Water Ice Clouds During Dust Storms Revealed From ExoMars Trace Gas Orbiter/NOMAD. *J. Geophys. Res. Planets*, 125(4). doi: 10.1029/2019JE006250
- Medvedev, A. S., Nakagawa, H., Mockel, C., Yiğit, E., Kuroda, T., Hartogh, P., ... Jakosky, B. M. (2016). Comparison of the martian thermospheric density and temperature from iuvs/maven data and general circulation modeling. *Geophys. Res. Lett.*, 43(7), 3095–3104. doi: 10.1002/2016GL068388
- Medvedev, A. S., & Yiğit, E. (2019). Gravity waves in planetary atmospheres: Their effects and parameterization in global circulation models. *Atmosphere*, 10(9). doi: 10.3390/atmos10090531
- Medvedev, A. S., Yiğit, E., Kuroda, T., & Hartogh, P. (2013). General circulation modeling of the martian upper atmosphere during global dust storms. *J. Geophys. Res. Planets*, 118, 1–13. doi: 10.1002/jgre.20163,2013
- Neary, L., Daerden, F., Aoki, S., Whiteway, J., Clancy, R. T., Smith, M., ... Vandaele, A. C. (2020). Explanation for the increase in high-altitude water on mars observed by nomad during the 2018 global dust storm. *Geophys. Res. Lett.*, 47(7). doi: 10.1029/2019GL084354
- Parish, H. F., Schubert, G., Hickey, M., & Walterscheid, R. L. (2009). Propagation of tropospheric gravity waves into the upper atmosphere of Mars. *Icarus*, 203, 28–37.
- Rafkin, S. C. R. (2009). A positive radiative-dynamic feedback mechanism for the maintenance and growth of Martian dust storms. *J. Geophys. Res. Planets*, 114(E1). doi: 10.1029/2008JE003217
- Randall, C. E., Carstens, J., France, J. A., Harvey, V. L., Hoffmann, L., Bailey, S. M., ... Russell, J. M. (2017). New AIM/CIPS global observations of gravity waves near 50–55 km. *Geophys. Res. Lett.*, 44(13), 7044–7052. doi: 10.1002/2017GL073943
- Shaposhnikov, D. S., Medvedev, A. S., Rodin, A. V., & Hartogh, P. (2019). Seasonal water “pump” in the atmosphere of Mars: Vertical transport to the thermosphere. *Geophys. Res. Lett.*, 46(8), 4161–4169. doi: 10.1029/2019GL082839
- Siddle, A., Mueller-Wodarg, I., Stone, S., & Yelle, R. (2019). Global characteristics of gravity waves in the upper atmosphere of Mars as measured by MAVEN/NGIMS. *Icarus*, 333, 12–21. doi: 10.1016/j.icarus.2019.05.021
- Terada, N., Leblanc, F., Nakagawa, H., Medvedev, A. S., Yiğit, E., Kuroda, T., ... Jakosky, B. M. (2017). Global distribution and parameter dependences of gravity wave activity in the martian upper thermosphere derived from maven/ngims observations. *J. Geophys. Res. Space Physics*. doi: 10.1002/2016JA023476
- Tolson, R., Keating, G., Zurek, R. W., Bougher, S. W., Justus, C. J., & Fritts, D. C. (2007). Application of accelerometer data to atmospheric modeling during mars aerobraking operations. *J. Spacecraft Rockets*, 44, 1172–1179.
- Vals, M., Spiga, A., Forget, F., Millour, E., Montabone, L., & Lott, F. (2019). Study of gravity waves distribution and propagation in the thermosphere of Mars based on MGS, ODY, MRO and MAVEN density measurements. *Planet. Space Sci.*, 178, 104708. doi: 10.1016/j.pss.2019.104708
- Vandaele, A. C., Korabiev, O., Daerden, F., Aoki, S., Thomas, I. R., Altieri, F., ... Rodionov, D. (2019). Martian dust storm impact on atmospheric H₂O and D/H observed by ExoMars Trace Gas Orbiter. *Nature*, 568(7753), 521–525. doi: 10.1038/s41586-019-1097-3
- Walterscheid, R. L., Hickey, M. P., & Schubert, G. (2013). Wave heating and jeans escape in the martian upper atmosphere. *J. Geophys. Res. Planets*, 118(2413–2422), 2169–9402. doi: 10.1002/jgre.20164
- Wu, Z., Li, T., Zhang, X., Li, J., & Cui, J. (2020). Dust tides and rapid meridional motions in the Martian atmosphere during major dust storms. *Nature Communications*, 11(1), 614. doi: 10.1038/s41467-020-14510-x
- Yiğit, E., Aylward, A. D., & Medvedev, A. S. (2008). Parameterization of the effects of vertically propagating gravity waves for thermosphere general circulation models: Sensitivity study. *J. Geophys. Res.*, 113. doi: 10.1029/2008JD010135

- Yiğit, E., England, S. L., Liu, G., Medvedev, A. S., Mahaffy, P. R., Kuroda, T., & Jakowsky, B. (2015). High-altitude gravity waves in the martian thermosphere observed by MAVEN/NGIMS and modeled by a gravity wave scheme. *Geophys. Res. Lett.*, *42*. doi: 10.1002/2015GL065307
- Yiğit, E., & Medvedev, A. S. (2019). Obscure waves in planetary atmospheres. *Physics Today*, *6*, 40-46. doi: 10.1063/PT.3.4226
- Yiğit, E., Medvedev, A. S., & Hartogh, P. (2018). Influence of gravity waves on the climatology of high-altitude martian carbon dioxide ice clouds. *Ann. Geophys.*, *36*(6), 1631–1646. doi: 10.5194/angeo-36-1631-2018
- Zurek, R. W., & Martin, L. J. (1993, February). Interannual variability of planet-encircling dust storms on Mars. *J. Geophys. Res. Planets*, *98*(E2), 3247–3259. doi: 10.1029/92JE02936

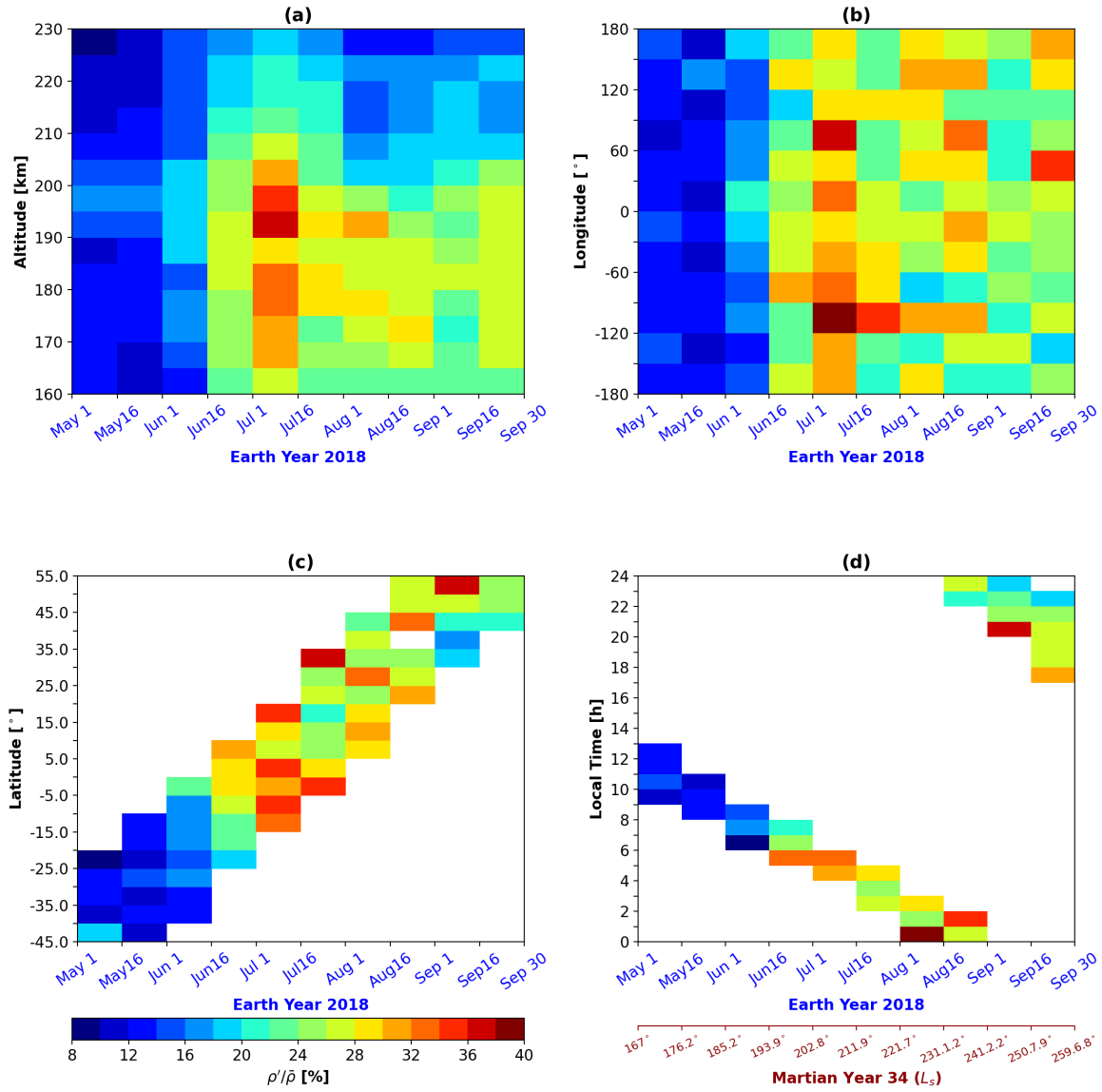


Figure 1. (a) Altitude, (b) longitude, (c) latitude, and (d) local time variations of the gravity wave activity in terms of relative carbon dioxide density perturbations $\rho'/\bar{\rho}$ before and during the different phases of the dust storm in MY=34 from solar longitudes $L_s = 167^\circ - 259^\circ$ (1 May-30 September 2018). All data are averaged over a ~ 15 -day time intervals. Data binning is performed in terms of 5 km, 30° , 5° , and 1 hour bins in (a)-(d), respectively.

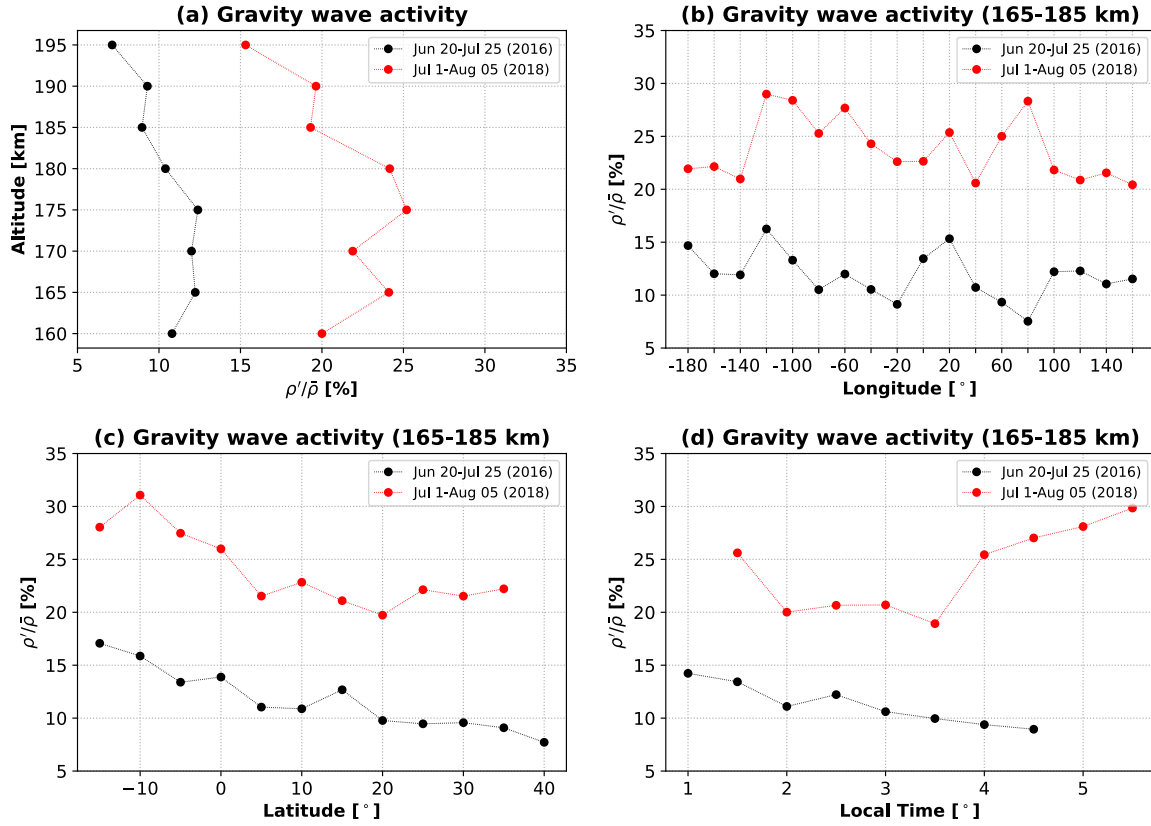


Figure 2. Comparison of gravity wave activity between the low-dust period in MY 33 $L_s = 171.7^\circ - 191.6^\circ$ (20 June – 25 July 2016) and dust storm period in MY 34, $L_s = 202.8^\circ - 224.2^\circ$ (1 July – 5 August 2018). (a) Altitude, (b) longitude, (c) latitude, and (d) local time variations of gravity wave activity under low dust conditions in 2016 and during the dust storm in 2018. The data is presented in terms of 5 km, 20° , 5° , and 0.5 hour bins in (a)-(d), respectively.

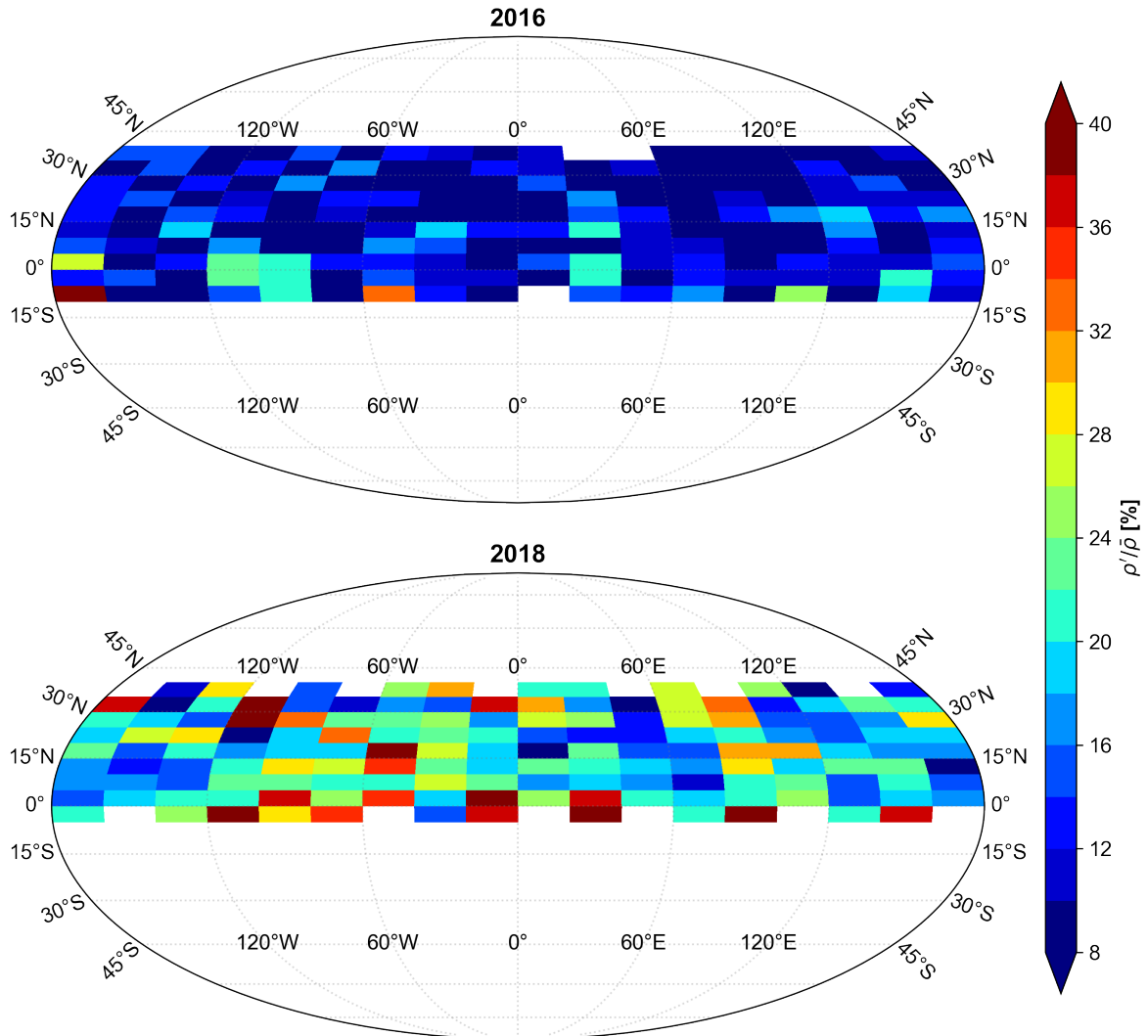


Figure 3. Comparison of the global distribution of the nighttime (1.5- 4.5 h) GW activity averaged within 165– 185 km between the low-dust period in 2016 (MY 33, $L_s = 171.7^\circ - 191.6^\circ$, 20 June-25 July 2016) and dust storm period in 2018 (MY 34, $L_s = 202.8^\circ - 224.2^\circ$, 1 July-5 August 2018) presented in Fig 2. The data is binned in 20° , 5° longitude-latitude bins.

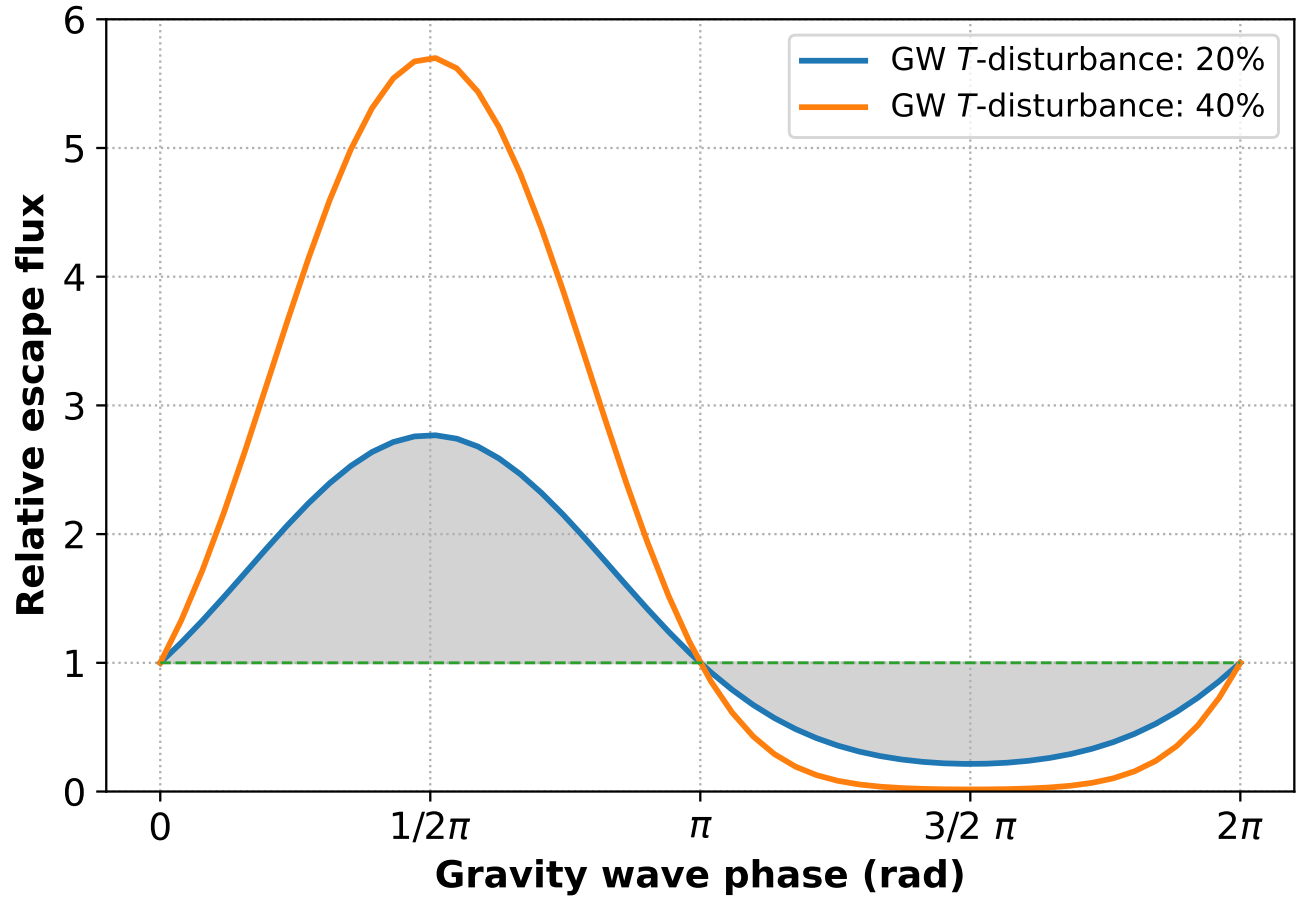


Figure 4. Relative escape flux $\frac{\phi(T+\delta T)}{\phi(T)}$ as a function of wave phase for the sinusoidally varying temperature disturbance δT . Blue and orange lines correspond to 20% and 40% amplitudes of fluctuations of the characteristic exobase temperature ($T_{exo} = 250$ K), correspondingly. The area under the curves gives the net (averaged over the entire wave phase) escape flux. Gray shading shows the net escape flux for 20% amplitude of disturbances.